Full data driven azimuthal inversion for anisotropy characterization

Mengmeng Zhang and Peter Mesdag, CGG*

Summary

A workflow of azimuthal inversion is presented and successfully applied on a wide-azimuth seismic dataset. This workflow is based on a novel approach to quantitatively extract anisotropy information in a horizontal transverse isotropic (HTI) medium. The method was first described by Mesdag (P. Mesdag, personal communication, 2016) and mimics anisotropic reflectivity behavior by isotropic forward modeling and anisotropy-transformed elastic properties (Mesdag, Debeye and Bornard, 2015). In this paper, a concept of an **A**zimuthally varying **L**ow **F**requency **M**odel (ALFM) is also introduced and demonstrated. The ALFM provides anisotropy information below seismic bandwidth, hereby reducing side-lobes of inverted magnitude of anisotropy, thus allowing better anisotropy characterization.

Introduction

Mesdag (P. Mesdag, personal communication, 2016) introduced a new approach of azimuthal inversion to quantitatively calculate and extract anisotropy magnitude and orientation information in an HTI medium. It defines anisotropy-transformed elastic properties, which allow us to apply isotropic modeling and inversion in anisotropic situations. Standard tools for performing modeling and inversion are applicable, which include wavelet estimation, well tying, low-frequency model building and azimuth-sectored pre-stack simultaneous inversion. Once azimuth-sectored inversion is completed, an Elastic Volumes Evaluation (EVE) tool, which is an advanced regression application with particular regression types modeling HTI anisotropy, is used to analyze azimuthally-oriented inverted elastic properties and predict anisotropy magnitude and orientation, i.e. layer properties-based anisotropy characterization.

Anisotropy input for the inversion comes solely from the seismic data. Due to the band-limited nature of seismic data, frequencies below the seismic band are missing in the predicted anisotropy magnitudes from a first pass of azimuthal inversion. Mesdag et al. (2010) showed that the missing low-frequency information in the low-frequency model results in artifacts in the inversion results (e.g., residual side lobes). Mesdag et al. (2010, 2015) presented ways of incorporating information extracted from the first pass inversion to update the low-frequency model in a quantitative, data-driven manner. In this paper we will extend this method to feed low frequencies of anisotropy extracted from a first pass azimuthal inversion back to the LFM. By inclusion of low frequencies of anisotropy in the LFM, i.e., building Azimuthally varying LFM (ALFM), side lobe artefacts of the inverted anisotropy magnitudes are removed, and the inverted anisotropy orientation is better determined and more stable. Interpretation of the updated inverted anisotropy is more consistent with interpretation of full-band inverted elastic properties, which makes the presence of anisotropy better explained in a physical and geological sense.

The workflow is illustrated with a case study on a wide-azimuth seismic dataset. Four wells drilled on the field were used in the study. Along with the illustration, several tips to successfully perform an azimuthal inversion are provided.

Method

The workflow consists of several steps which can be grouped into three parts: data preparation, first pass inversion and low-frequency model update. In data preparation, the seismic data first need to be aligned in the offset, angle and azimuth directions. Then seismic feasibility studies need to be conducted to ensure the lateral consistency of seismic amplitudes and verify that there are quantifiable differences in seismic amplitudes from one azimuthal sector to another. In the first pass inversion, no attempt is made to update frequencies below the seismic band in the azimuth sense, as a single low-frequency model is used for estimation of each elastic parameter in all azimuth sectors. This first pass inversion does include well tying, wavelet estimation, 3D low frequency model building, a full-azimuth pre-stack inversion, several azimuthally-oriented pre-stack inversions and initial anisotropy prediction based on the first pass azimuth-sectored inversion results. The anisotropy result from the first pass inversion is band limited. In the third part of the workflow, the low-frequency model update, inverted anisotropy information is fed back to low-frequency models to enrich the low frequencies in the azimuth sense. The azimuth-sectored inverted elastic properties from the first pass inversion are updated either by directly replacing low frequencies with updated low frequencies from an azimuthally-varying LFM or by performing azimuth-sectored pre-stack inversions with new azimuthally-varying low-frequency models. After this, anisotropy is re-calculated based on the updated inverted elastic properties. The low frequency update can be an iterative procedure.

Examples

This workflow is successfully applied on a wide-azimuth seismic dataset. Figure 1 shows the distribution of offset

and azimuth. As full-azimuth coverage is needed for an anisotropy study, the far offset with limited azimuth coverage are excluded during data preparation. For the nearest offset, azimuth coverage is very sparse. As azimuthal anisotropy effects mainly manifest themselves on far angles/ offsets (Rüger, 1998), tiles of the nearest offset can be stacked together as a full-azimuth stack and used as the nearest partial stack for every azimuthal sector. For unbiased analysis of the expected azimuthal behavior, a minimum of 6 azimuth sectors is required.

Seismic alignment in both the angle/offset and the azimuth directions need to be carefully performed. Please note that even though anisotropic move out and anisotropic velocity correction may have been applied during processing, residual time alignment in both angle/offset and azimuth directions are generally necessary. Lateral variation of seismic amplitude needs to be checked to ensure that it is not due to acquisition or processing artifacts, otherwise it needs to be compensated prior to or during inversion. As time alignment and lateral amplitude consistency are standard seismic QC steps for pre-stack simultaneous inversion, they will not be discussed in detail in this paper. For this study, 6 azimuthal sectors and 5 partial stacks within each azimuth sector were created.

Before performing 6 azimuth-sectored pre-stack inversions, a pre-stack inversion based on full-azimuth stacked seismic was performed. This full-azimuth inversion provides a first elastic properties estimate and also offers a 'best' inverted P-impedance. This full-azimuth P-Impedance is used as a hard constraint for each of the azimuth-sectored inversions, as in theory, P-impedance should not show any azimuthal variation. In our current technique, it is assumed that azimuthal variations in the seismic amplitudes are due to azimuthal variation in reflectivity rather than in the wavelet, i.e. if we could have azimuthally-oriented well logs, the wavelets estimated from different azimuth-sectored seismic should be the same. Wavelet estimation is based on full-azimuth seismic and logs in vertical boreholes. Ideally, for a HTI situation, the seismic from the isotropic plane should be used together with logs in vertical boreholes to estimate the wavelets, but at this stage, we may lack reliable azimuthal information. For weak anisotropy, we assume the wavelet amplitude bias, which comes from replacing seismic in an isotropic plane with full-azimuth seismic, is second order compared with the azimuthal variation of reflectivity being studied. More accurate wavelet estimation may be achievable once you have information on the azimuth of anisotropy after the first pass of inversion.

As the same reflector does not change its position azimuthally, well tying only needs to be performed once. For the first pass inversion a 3D earth model is built based on interpolation of vertical logs and then used as a single LFM for all azimuth-sectored inversions, i.e. frequencies below the seismic band of inverted properties are the same for all sectors. Thus the calculated anisotropy which is based on analysis of the azimuthal variation of the inverted elastic properties lacks low frequencies. Figure 2 shows a

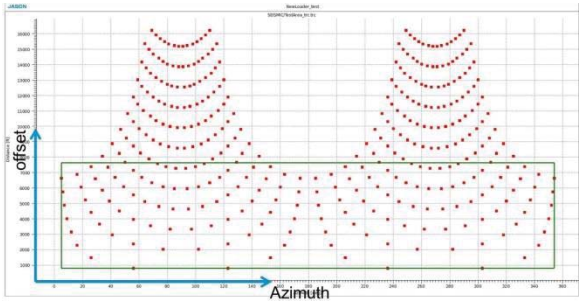

Figure 1: A 'necklace' plot shows the offset and azimuth coverage of a survey. Due to the acquisition configuration, the azimuth coverage of very far offset is relative poor. Full-azimuth coverage is shown within the green box. Though the offset in the survey can go up to 16000 feet, the largest offset used for inversion is limited to approximately 7500 feet.

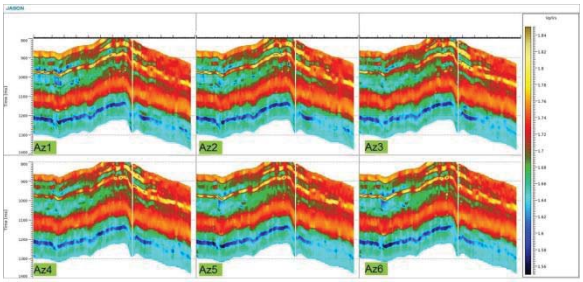

Figure 2: Cross sections of inverted effective Vp/Vs from six azimuthally independent pre-stack inversions (a single LFM is used for all azimuthal sectors).

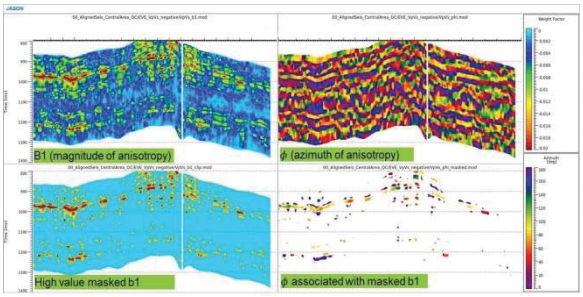

Figure 3: Cross sections of inverted anisotropy amplitude (upper left) and anistropy orientation (upper right) which is the azimuth of symmetry axis. The lower left panel displays high anisotropy masked areas, and the lower right panel displays the azimuth associated with high anisotropy areas. Light blue represents an anisotropy amplitude of zero, its corresponding azimuth is undefined as anisotropy orientation is only resolvable if there is sufficient anisotropy magnitude.

cross section of inverted Vp/Vs for six azimuth sectors. The two panels at the top of figure 3 are displaying calculated anisotropy magnitude and anisotropy orientation based on the inverted Vp/Vs shown in figure 2. Due to the method used to estimate anisotropy, which is detailed by Mesdag (P. Mesdag, personal communication, 2016), side lobe effects in anisotropy magnitude, which result from the **lack of low frequencies in azimuth variation**, lead to a 90-degree flip in anisotropy orientation, which is shown as lateral striping in orientation sections. Figure 4 is an analogy illustrating the side lobe effects of inverted results when the low frequencies are missing.

In theory, anisotropy can also be calculated from the inverted effective density. However, in practice, seismic angles of at least 45 degrees are required in order to independently invert for density by pre-stack inversion. For this data set the seismic angles at the reservoir level go up to 30 degrees only, which means that the effective density is actually not independently resolvable.

For the azimuthal low-frequency model update, we try to enrich the low frequencies of the azimuthal variation of the inverted effective elastic properties. As anisotropy can be reliably resolved only if its effects are large enough, a threshold is applied to the predicted anisotropy amplitudes, i.e. the anisotropy amplitude will be reset to zero if it is smaller than the threshold. The lower left panel in figure 3 shows the masked anisotropy magnitudes, and the lower right panel displays the corresponding anisotropy orientations associated with areas of high anisotropy magnitudes. Next, a most likely azimuth corresponding to a high anisotropy layer is identified based on statistical analysis, as azimuth should not vary significantly within a single geological setting. Figure 5 highlights two high-anisotropy layers. The most likely azimuth is chosen for each layer based on the peak of the histogram associated with high anisotropy. With the most likely azimuth and masked magnitudes, the anisotropy predicted from the first pass inversion is fed back into the azimuth-sectored inversions as an ALFM. This enriches the low frequencies of the azimuthal variation of inverted elastic properties. This process is fulfilled by transforming the initial single LFM to azimuthally-varying low-frequency models with a transform equation introduced by Mesdag et al. (2015):

$$\left(\frac{V_p}{V_s}\right)' = \left(\sqrt{\delta_r}\gamma_r\right)^{\cos^2(\omega-\varphi)} \cdot \left(\frac{\varepsilon_r}{\delta_r}\right)^{\frac{4k-1}{8k}\cdot\cos^4(\omega-\varphi)} \cdot \frac{V_p}{V_s} \qquad (1)$$

given

$$\cos^2(\omega-\varphi) \approx \cos^4(\omega-\varphi)$$

Equation 1 can be approximated as:

$$\left(\frac{V_p}{V_s}\right)' \approx e^{2b_1 * cos^2(\omega-\phi)} \cdot \frac{V_p}{V_s} \qquad (2)$$

where

$$b_1 = \frac{1}{2}\log\sqrt{\delta_r}\gamma_r + \frac{1}{2}\frac{4K-1}{8K}\log\frac{\varepsilon_r}{\delta_r}$$

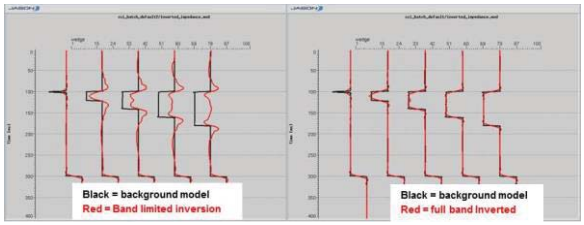

Figure 4: Cross sections illustrate the side lobe effects (left) on inverted results when low frequencies are missing in inversion. The picture on the right shows side lobes are removed if the correct low-frequency model is included in inversion.

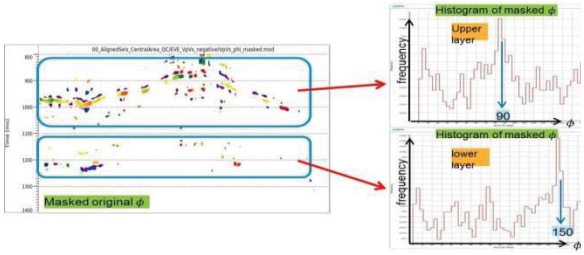

Figure 5: Left section displays azimuth associated with high anisotropy, two separate layers are indicated with two blue boxes. Two pictures on the right illustrate how the most likely azimuth is identified for each layer based on the histogram of masked azimuth.

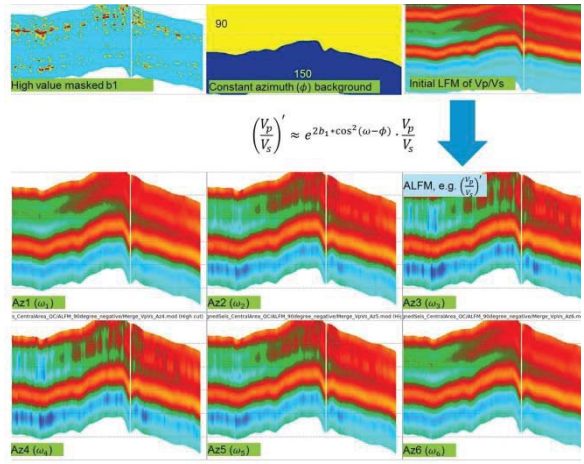

Figure 6: Transformation from an initial single LFM to azimuthally-varying low-frequency models with the transform equation and predicted anisotropy from the first pass inversion.

Figure 6 illustrates this transformation: the initial single LFM of Vp/Vs is equivalent to the isotropic Vp/Vs on the right side of equation 2. The identified most likely azimuth is the azimuth of symmetry axis, i.e. ϕ in the equation. The azimuth values of the different azimuthal sectors represent the survey azimuth, i.e. ω in the equation. The masked anisotropy magnitudes denote the b_1 values. (The logarithm

of equation 2 is analyzed by the Elastic Volumes Evaluator) The azimuthally varying low frequency models of Vp/Vs are transformed to effective Vp/Vs (i.e., $\frac{V_p}{V_s}'$ on the left side of equation).

Once the azimuthally-varying low-frequency models are obtained, the inverted effective elastic properties can be updated either by directly replacing the original low frequencies with updated azimuthally-varying low frequencies or performing azimuthally-oriented pre-stack inversions once more with the AFLM as trends. The final step is to apply the Elastic Volumes Evaluator to the updated effective properties to re-calculate anisotropy magnitudes and orientations. Figure 7 shows a cross section comparison between anisotropy amplitudes predicted from the first pass inversion and anisotropy amplitudes re-calculated from updated effective Vp/Vs. The side lobe effects due to the lack of low frequencies in the azimuthal variation, in the left panel (black ovals) have been well removed in the right panel. Statistical analysis of the updated orientation information is illustrated in figure 8. When compared with the similar analysis shown in figure 5, it is clear that the orientations are better centered at a single peak instead of at two peaks which happen to be around 90 degrees apart. This confirms again that side lobes effects have been well removed. Figure 9 shows a comparison between a cross section of inverted anisotropy magnitude and full-azimuth seismic inverted Vp/Vs. The black arrows pointing upwards indicate a high anisotropy layer corresponding to a high Vp/Vs layer. The area within the oval, the high-anisotropy area, can correspond to both high and low Vp/Vs layers. The area within the oval is located at a structural high position which might have introduced additional fracturing. This kind of pattern-matching of elastic properties to anisotropy, to some extent, may provide a physical explanation for high-anisotropy areas. The lateral consistency of the anisotropy can be better examined by horizon extractions. Note that a horizon going through a high-anisotropy layer might not be the same as a horizon interpreted based on seismic reflectivity data. Figure 10 shows a comparison between a horizon extraction of inverted anisotropy amplitudes (left) and orientation (right). It can be concluded that at this level the dominant orientation of high-anisotropy (red color in the left panel) throughout the whole survey is around 90 degrees (yellowish in the right panel), corresponding well with the dominant stress orientation in this area.

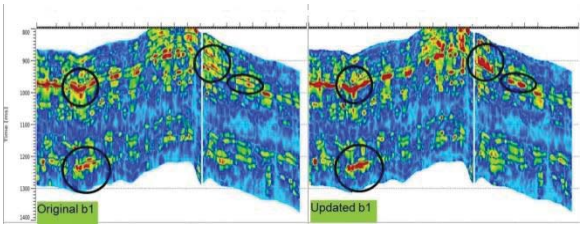

Figure 7: Comparison between ansitropy amplitudes from the first pass inversion (left) and anisotropy amplitudes re-calculated from updated effective Vp/Vs (right).

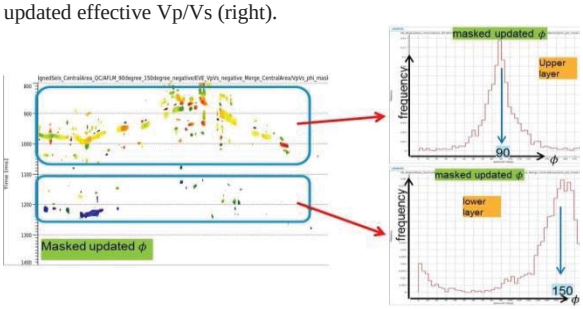

Figure 8: Left picture displays azimuths associated with high-anisotropy from updated effective Vp/Vs. The two pictures on the right show histograms of high anisotropy-masked azimuths in two separate layers.

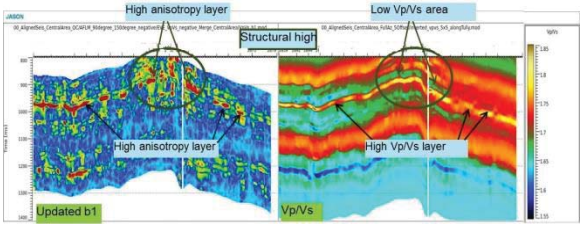

Figure 9: The left panel shows a cross section of predicted anisotropy magnitude. The right panel shows a cross section of full-azimuth seismic inverted Vp/Vs, on the same tracegate.

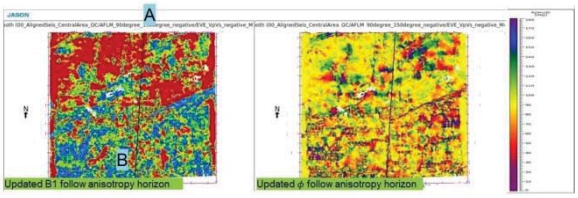

Figure 10: Horizon extraction of anisotropy magnitude (left panel) and anisotropy orientation (right panel).

Conclusion

A workflow of layer property-based full band anisotropy estimation is presented. The missing low frequencies of anisotropy are introduced by azimuthally varying low frequency models. As the azimuthal variation of these ALFMs is solely based on the first pass inversion, a fully seismic data driven anisotropy characterization is achieved.

Acknowledgement

We would like to acknowledge CGG multi-client for permission to show the data.

EDITED REFERENCES

Note: This reference list is a copyedited version of the reference list submitted by the author. Reference lists for the 2016 SEG Technical Program Expanded Abstracts have been copyedited so that references provided with the online metadata for each paper will achieve a high degree of linking to cited sources that appear on the Web.

REFERENCES

Mesdag, P., H. Debeye, and R. Bornard, 2015, Method and device for the generation and application of anisotropic elastic parameters in horizontal transverse isotropic (HTI) media: Patent WO2015014762 A2.

Mesdag, P. R., D. Marquez, L. de Groot, and V. Aubin, 2010, Updating low frequency model: 72nd Annual International Conference and Exhibition, EAGE, Extended Abstracts, http://dx.doi.org/10.3997/2214-4609.201400777.

Mesdag, P. R., M. R. Saberi, C. Mangat, and P. Geoph, 2015, Time lapse data driven low frequency model update: 85th Annual International Meeting, SEG, Expanded Abstracts, 5498–5502, http://dx.doi.org/10.1190/segam2015-5797567.1.

Rüger, A., 1998, Variation of *P*-wave reflectivity with offset and azimuth in anisotropic media: Geophysics, **63**, 935–947, http://dx.doi.org/10.1190/1.1444405.